ELSEVIER

### Contents lists available at ScienceDirect

# Surface Science

journal homepage: www.elsevier.com/locate/susc





# DRIFTS investigation of toluene oxidation on CeO<sub>2</sub> nanoparticles<sup>★</sup>

Paul K. Huttunen, Daniela Labadini, Genevieve Asselin, Sabrina S. Hafiz, Sumeyra Gokalp, Maria D. Kipreos, Michelle Foster \*

Department of Chemistry, University of Massachusetts Boston, Boston, MA 02125, United States

# ARTICLE INFO

Keywords:
DRIFTS
Ceria
Catalytic combustion toluene
Surface hydroxyls
Toluene oxidation

#### ABSTRACT

The oxidation mechanism of toluene on the surface of heat-treated  $CeO_2$  nanoparticles was investigated using diffuse reflectance infrared Fourier transform spectroscopy (DRIFTS). When introduced to the  $CeO_2$  surface, toluene either chemisorbs to an oxygen bound to a single cerium atom creating monobound (m) benzyloxy or to an oxygen bound to two neighboring cerium atoms forming bridged (b) benzyloxy. From the DRIFTS analysis, benzoate production is directly dependent on the presence and oxidation of b-benzyloxy groups. Using temperature dependent peak height analysis of the DRIFTS spectra, the oxidation state of specific  $v_s(OCO)$  bands of bidentate (bdt) benzoate groups are identified through pairing with their  $v_a(OCO)$  counterparts. Surface lattice oxygens and b-hydroxyl groups are found to facilitate the chemisorption of toluene as the two surface benzyloxy groups. Once toluene reacts with the substrate, surface hydroxyls react with m-benzyloxy groups to create additional b-benzyloxy groups as well as enabling the transformation of b-benzyloxy groups to bdt-benzoate groups. The previously unclear intermediate transformation steps of toluene to bdt-benzoate on the surface of  $CeO_2$  and surface hydroxyls species role in said transformation is unveiled through the use of peak height analysis of the collected DRIFTS spectra.

### 1. Introduction

Toluene is a highly utilized, volatile organic compound (VOC) considered to be a strong pollutant due to its high volatility, developmental toxicity, nervous system effects, and environmental impact [1-3]. Catalytic combustion is a well-established VOC remediation technique where VOC gasses are fully oxidized with higher conversion rates and selectivity as well as lower energy requirements compared to traditional combustion [4-7]. The catalytic combustion of toluene results in the full oxidation of toluene over a solid catalyst into less harmful and more manageable  $H_2O$  and  $CO_2$  [6,8].

 ${\rm CeO_2}$  (ceria) has garnered a great deal of attention as an ideal catalyst and support for the catalytic combustion of VOCs, including toluene, due to its oxygen storage potential and ability to resist sintering which increases the efficiency and selectivity of traditional noble metal catalysts [9]. The surface of ceria is the location of toluene's oxidation to benzoate in ceria based/supported catalysts, an important process in the full oxidation of toluene [10–12]. Previous studies have proposed that the catalytic combustion of toluene over ceria based/supported and

similar catalysts follows the Mars-Van Krevelen (MVK) mechanism [7,9, 12–17] in that components found in the products originate from the solid catalyst [18,19]. Following the MVK mechanism for the catalytic combustion of toluene, oxygen from the substrate is incorporated into the produced CO<sub>2</sub> and H<sub>2</sub>O; but the true mechanism has yet to be fully characterized.

Diffuse reflectance infrared Fourier transform spectroscopy (DRIFTS) is a powerful tool used for analyzing *in situ* substrate/adsorbate interactions [20–27]. A small handful of studies have employed DRIFTS analysis in an attempt characterize the true mechanism for the oxidation of toluene on the surface of ceria and ceria based/supported catalysts [11,12,28]. From these endeavors, benzaldehyde and benzoate have been proposed as intermediates, forming on ceria during the full oxidation of toluene. The methyl group of toluene is proposed to chemisorb to the surface of ceria forming benzaldehyde [11,28]. However, there are competing theories on the production of benzoate in similar catalytic systems that hint at benzyloxy being another potential precursor to benzoate [29,30]. There is also doubt about the presence of benzaldehyde as an intermediate during toluene oxidation due to the

E-mail address: michelle.foster@umb.edu (M. Foster).

<sup>\*</sup> This article is part of the "Young Investigator Special Issue 2022". The CV of the first author can be found under link - https://ars.els-cdn.com/content/image/1-s2.0-S0039602822000279-mmc1.pdf.

<sup>\*</sup> Corresponding author.

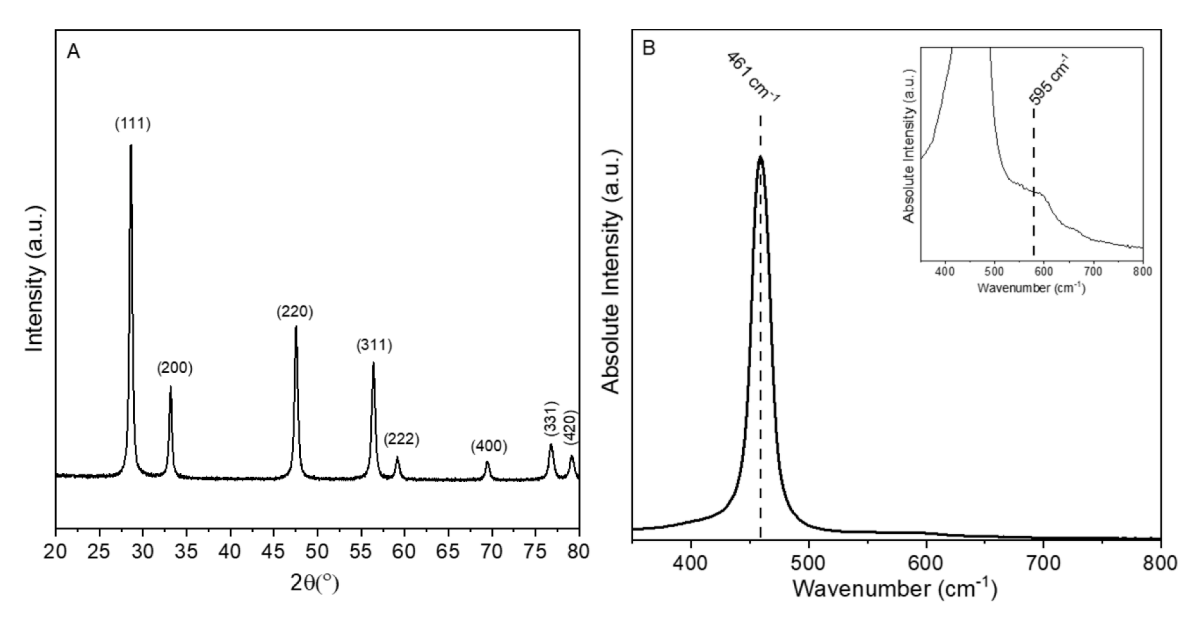


Fig. 1. (A) XRD pattern of as-purchased CeO<sub>2</sub> and (B) Raman crystallinity analysis of as-purchased CeO<sub>2</sub>. Inset is the same spectrum multiplied by 19.5 to show defect features.

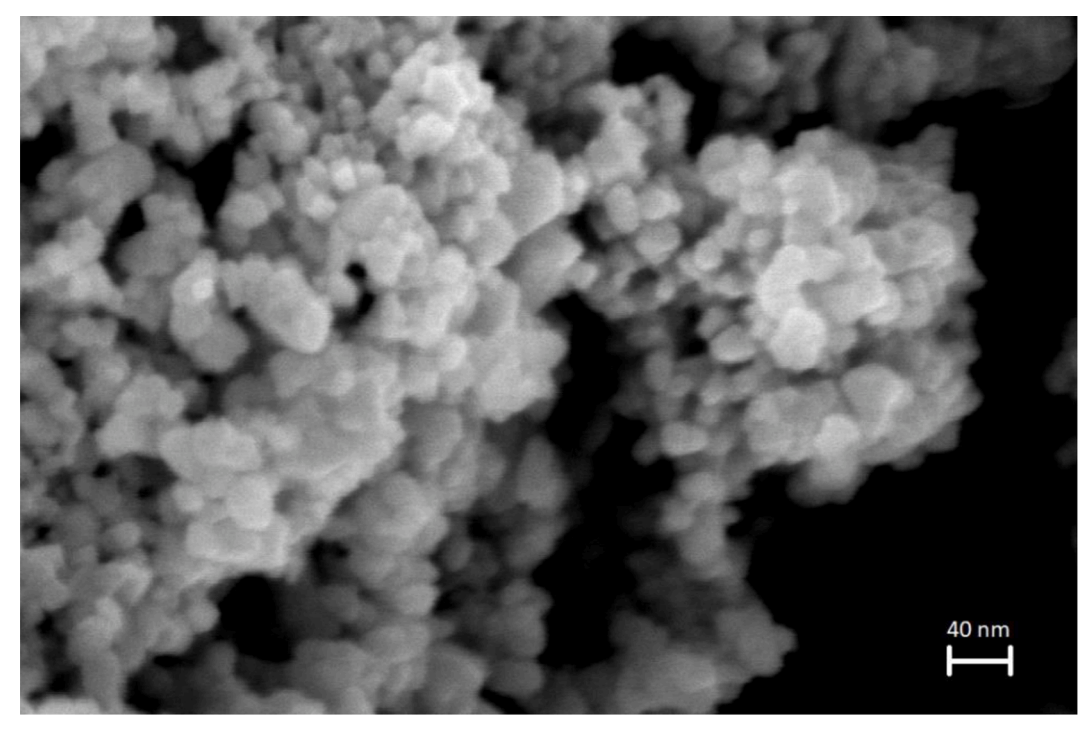


Fig. 2. Scanning electron micrograph of  ${\sf CeO}_2$  nanoparticles.

lack of carbonyl features during DRIFTS studies of the catalytic combustion of toluene over ceria [11]. In addition to the intermediate pathway disagreements, surface hydroxyls are reported to be active in the binding and catalytic conversion of VOCs but in depth attempts to catalog their role in the oxidation of toluene over ceria are largely absent [31–36]. These OH species are potential sources of oxygen during the oxidation of toluene to benzoate supporting the need for a concentrated analysis of hydroxyl reactivity.

In this study, evacuated *in situ* DRIFTS is used to observe the surface chemistry of  $CeO_2$  after toluene introduction and during the transformation of intermediate species as a function of temperature [37]. In tandem with the *in situ* DRIFTS studies, relative peak height analysis is

utilized to relate benzoate symmetric and asymmetric OCO stretching features to one another and to catalog the transformation of toluene to benzoate as a function of temperature. In this manner, a detailed mechanism of the oxidation of toluene to benzoate on ceria is established.

### 2. Experimental

### 2.1. Catalyst characterization

Ceria nanoparticles (50 nm) were purchased from Sigma Aldrich. The crystallinity of the  ${\rm CeO_2}$  was verified via PXRD and Raman

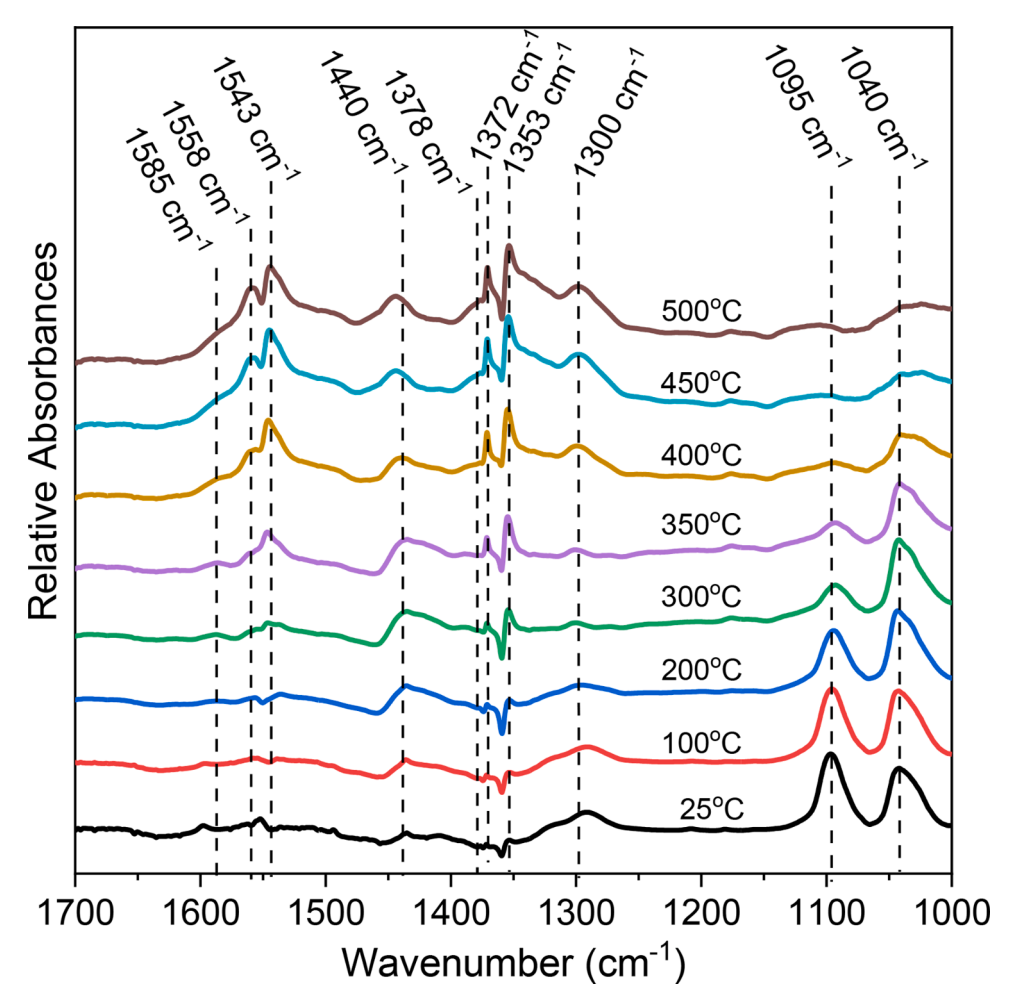


Fig. 3. Difference DRIFTS of the carbon-oxygen stretching and carbon-hydrogen bending region of the ceria surface after reaction with toluene as a function of temperatures.

spectroscopy. A Bruker D2 Phaser using CuK $\alpha$  radiation (1.54184 Å) was used to collect the XRD pattern of CeO $_2$  and is presented in Fig. 1A. Diffraction patterns were recorded over a 2 $\theta$  range of 20–80°, using a step size of 0.02° and a step time of 0.5 s. The intensive diffraction peaks of CeO $_2$  are observed at 2 $\theta$  = 28.6°, 33.1°, 47.5°, 56.4°, 59.1°, 69.5°, 76.8°, and 79.2° and attributed to the (111), (200), (220), (311), (222), (400), (331), and (420) plane diffractions of the fluorite structure of CeO $_2$  [JCPDS PDF 34–0394]. The Raman spectrum of CeO $_2$  was collected with a Bruker SENTERRA II confocal Raman Microscope using the 532 nm laser at 2.5 mW with a 9–15 cm $^{-1}$  resolution and is presented in Fig. 1B. As shown in Fig. 1B, two distinct Raman modes are present at 461 cm $^{-1}$ , the F $_2$ g band, indicating the 8 coordinated Ce and 4 coordinated O of the Ce $^{-0}$ 0 stretch characteristic of fluorite structured ceria, and 595 cm $^{-1}$ 1 representing the Ce $^{3+}$ 4 defect [38,39].

The size of the ceria nanoparticles was verified by scanning electron microscopy (Zeiss Sigma 500 VP) using an in-lens detector and an accelerator voltage of 3.00 kV. The SEM image of the  $\text{CeO}_2$  nanoparticles is presented in Fig. 2 and depicts particles with an average diameter of 40–50 nm.

# 2.2. Catalyst preparation and DRIFTS analysis

Infrared spectra (128 scans, 2 cm<sup>-1</sup> resolution) were collected using a Nicolet iS 50 FT-IR spectrometer (Thermo Fisher Scientific, MCT-High D\* detector) equipped with a Praying Mantis diffuse reflectance accessory (Harrick Scientific). A high temperature reaction chamber (Harrick Scientific, HTRC) was situated within the Praying Mantis accessory

inside the sample compartment of the FTIR, which was under constant  $N_2$  purge, and used to perform in situ DRIFTS experiments. The aspurchased ceria powder was placed on wire mesh made of stainless-steel in a sample holding cup within the HTRC, which was connected to a gas handling manifold with a base pressure of  $10^{-5}$  torr. A type K thermocouple was inserted into the HTRC in a designated compartment in contact with the sample holder to monitor the temperature of the substrate. The ceria sample was heated at 500  $^{\circ}\text{C}$  under high vacuum for 16 h. The ceria sample was then cooled to room temperature and a spectrum of the cleaned ceria at 25  $^{\circ}\text{C}$  was taken and used as a background to create difference pseudo-absorbance spectra, allowing for a clear view of the changes to the surface during reactions.

The gas handling manifold was charged with 0.1 torr of HPLC grade toluene (Sigma Aldrich, freeze, pumped, and thawed) and introduced to the ceria sample at 25 °C until the surface chemistry stabilized as monitored with DRIFTS. Once surface chemistry stabilized a final DRIFTS scan was taken to record the surface species and the HTRC and gas handling manifold were pumped down to base pressure and the remaining experiments were performed with the system under high vacuum. The temperature of the sample was then increased to  $100~^{\circ}$ C and held at that temperature until surface chemistry stabilization, once again taking DRIFTS spectra to monitor the reaction, when the final surface spectra was recorded. This method was continued at  $100~^{\circ}$ C increments up to  $300~^{\circ}$ C then  $50~^{\circ}$ C increments to fully observe the fine feature changes at temperatures from  $300~^{\circ}$ C to  $500~^{\circ}$ C. The spectra were reprocessed using a spectrum of a gold foil mirror (Alfa Aesar) in the evacuated HTRC as the background to record the absolute pseudo-

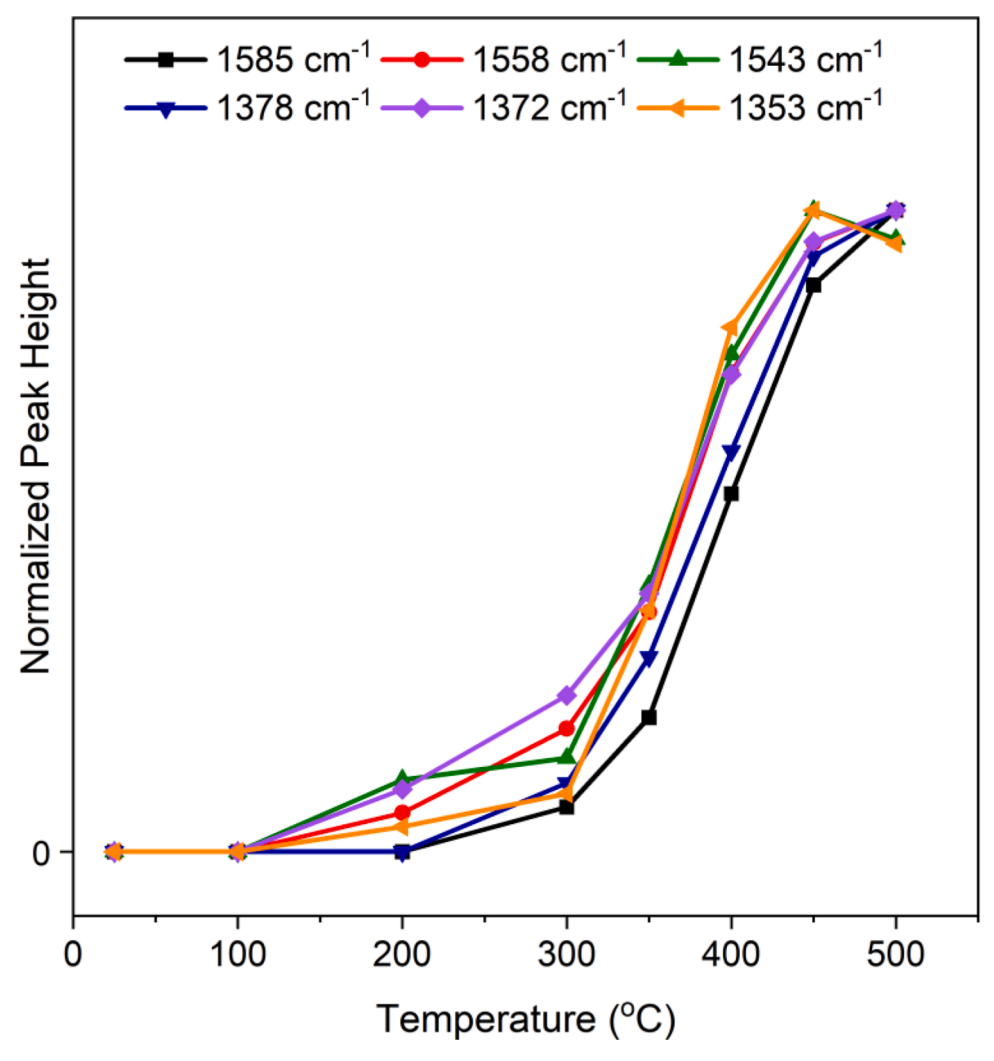


Fig. 4. Temperature dependent normalized peak height analysis of benzoate features.  $v_a(OCO)$ : bdt-benzoate (33) (1585 cm<sup>-1</sup>), bdt-benzoate (43) (1558 cm<sup>-1</sup>), bdt-benzoate (44) (1543 cm<sup>-1</sup>), and  $v_s(OCO)$ : bdt-benzoate (33) (1378 cm<sup>-1</sup>), bdt-benzoate (43) (1373 cm<sup>-1</sup>), bdt-benzoate (44) and (1353 cm<sup>-1</sup>).

absorption spectrum. While the difference spectrum obtained from using the cooled ceria as a background is useful for accurately visualizing the changes that occur in the region where carbonate and alkoxy species are observed, the absolute pseudo-absorption spectrum is more useful for monitoring hydroxyl reactivity.

### 2.3. Relative peak height analysis

The peak heights of the features of interest from the absolute pseudo-adsorption spectrum were recorded as a function of temperature. The heights of individual features were normalized (0, 1) over the temperature range and plotted as a function of temperature. Normalization allows the changes in intensities of different peaks to be seen on the same scale, which aids in the visualization of relationships between different surface features. In addition, normalized peak heights more accurately represent the percent change in intensity a feature undergoes over the course of the heat treatment.

## 3. Results and discussion

# 3.1. DRIFTS study

# 3.1.1. Carbon-oxygen intermediate DRIFTS characterization

In order to identify the mechanism for the oxidation of toluene over ceria, difference DRIFTS spectra are utilized to observe the system after

0.1 torr of toluene is introduced followed by evacuation and subsequent heating from 25 to 500 °C. As depicted in Fig. 3, with the addition of toluene at 25 °C intense bands associated with the  $\nu$ (CO) of monobound (m) alkoxy species at 1095 cm<sup>-1</sup> and the  $\nu$ (CO) of bridged (b) alkoxy species at 1040 cm<sup>-1</sup> are formed [20,23,30,37,40] through the chemisorption of toluene on ceria via methyl group and surface oxygen interaction; the alkoxy species is identified as benzyloxy [30,41,42]. At 25 °C, a band at 1435 cm<sup>-1</sup> also appears, representative of the aromatic ring vibration of the adsorbed phenyl group [11,37,42]. However, as temperature increases past 100 °C a new more intense band centered at  $1440~{\rm cm}^{-1}$ , representing carbonate, forms and overshadows the 1435cm<sup>-1</sup> feature. The 1290 cm<sup>-1</sup> band that is observed at 25 °C and decreases until 300 °C is associated with the CH2 deformation vibration of alkoxy species, additionally supporting the presence of benzyloxy species [29,43-45]. At 300 °C and above a band at 1300 cm<sup>-1</sup>, also associated with carbonate features, forms and continues to grow until 500 °C is reached, further supporting the formation of surface carbonate [46–48]. Above 100 °C three distinct bands at 1585 cm<sup>-1</sup>, 1558 cm<sup>-1</sup> and 1543 cm<sup>-1</sup>, associated with the  $v_a(OCO)$  benzoate species with unique binding site oxidation states, appear and increase in intensity with temperature [11,20-22,28-30,37,46]. The band at 1543 cm<sup>-1</sup> is associated with bidentate carboxylate species bound to two  $\mathrm{Ce}^{4+}$  atoms (bdt-benzoate (44)), 1558 cm<sup>-1</sup> with bdt-carboxylate species bound to one Ce<sup>4+</sup> atom and one Ce<sup>3+</sup> atom (bdt-benzoate (43)), and 1585 cm<sup>-1</sup> with bdt-carboxylate species bound to two Ce3+ atoms (bdt-benzoate

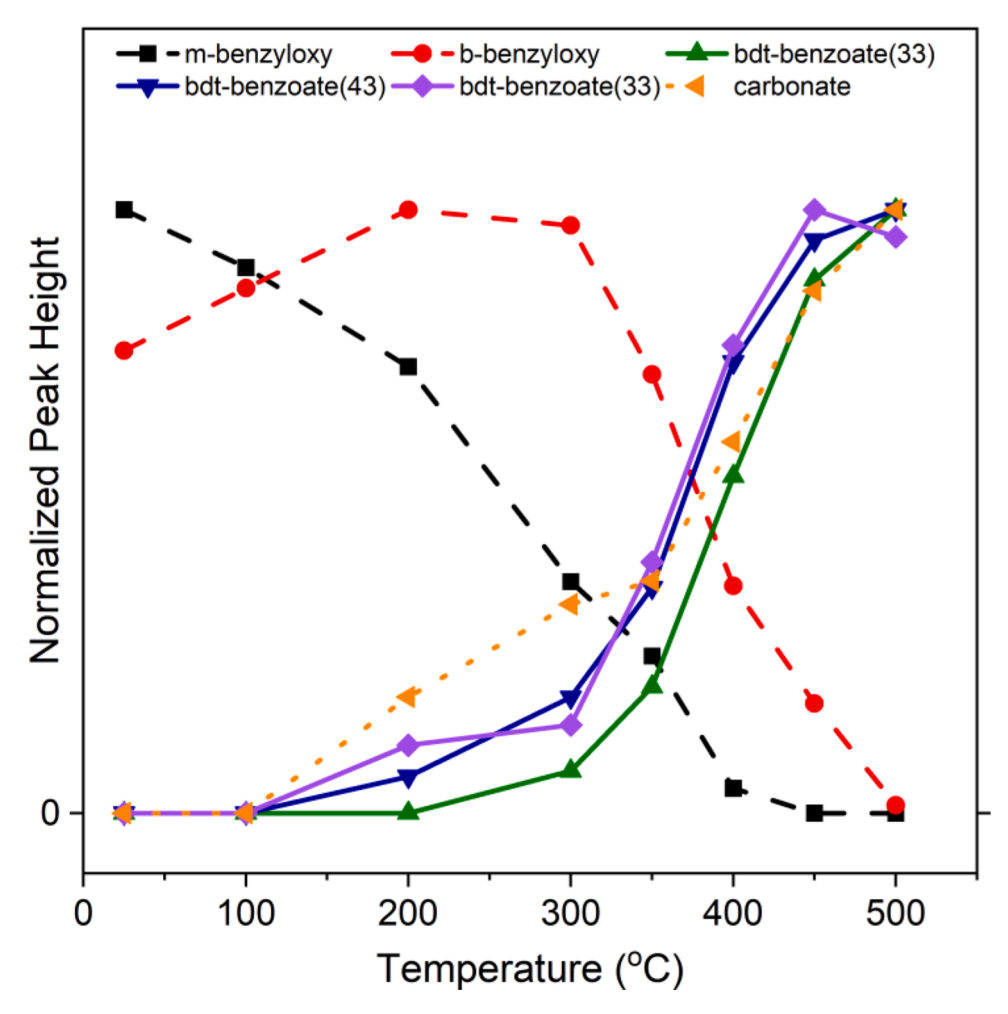


**Fig. 5.** Temperature dependent normalized peak height analysis of benzyloxy (- -), benzoate (−), and carbonate (⋯) features. m-benzyloxy (1095 cm<sup>-1</sup>), b-benzyloxy (1040 cm<sup>-1</sup>), bdt-benzoate (33) (1585 cm<sup>-1</sup>), bdt-benzoate (43) (1558 cm<sup>-1</sup>), bdt-benzoate (44) (1543 cm<sup>-1</sup>), and carbonate (1440 cm<sup>-1</sup>).

(33)) [11,20–22,28–30,37,46]. The bands at 1378 cm $^{-1}$ , 1373 cm $^{-1}$ , and 1353 cm $^{-1}$  are associated with the  $\nu_s(OCO)$  of carboxylate, in this case benzoate [11,28,37,46,48,49]. The m-benzyloxy, b-benzyloxy, and three bdt-benzoate species are illustrated in Scheme 1.

From the DRIFTS spectra depicted in Fig. 3 the m-benzyloxy and bbenzyloxy bands at 1095 cm<sup>-1</sup> and 1040 cm<sup>-1</sup> respectively are observed at 25 °C. The m-benzyloxy features decrease at temperatures above 25  $\,$ °C while the b-benzyloxy features increase up to 200 °C and begin to decrease at 300  $^{\circ}$ C. The 1435 cm $^{-1}$  band that represents the aromatic ring vibration is observed at 25 °C and 100 °C and is overshadowed by the 1440 cm<sup>-1</sup> band of carbonate species at 200 °C and higher. Carbonate species are likely forming as the phenyl group on benzoate is separated allowing for further oxidation of the carboxylate group. The  $1290~\text{cm}^{-1}$  band associated with the  $\text{CH}_2$  deformation vibration of benzyloxy species decreases until 200 °C as benzyloxy species are lost through desorption or transformation when it is overtaken by the 1300 cm<sup>-1</sup> carbonate band that increases in intensity at temperatures >300 °C [29,43–45]. A faint shoulder at 1462 cm<sup>-1</sup> that appears at temperatures >400 °C is associated with methylene and potentially indicates ring breakage on the catalytic surface [30,50]. The ring separation is supported by the previously mentioned presence of carbonates that would allow the ring to interact directly with the catalytic surface. The difference in peak position of the asymmetric/symmetric OCO bands being more than 100 cm<sup>-1</sup> and less than 300 cm<sup>-1</sup> further confirms the bidentate binding mode [11,20,21,40,51]. The bands at 1543, 1558, and 1585 cm<sup>-1</sup> that represent carboxylate species bound to metal centers with different oxidations states are well established and identified as,

bdt-benzoate (44), bdt-benzoate (43), and bdt-benzoate (33), respectively. However, their sister  $\nu_s(OCO)$  bands are not as precisely defined [20,21,46]. In order to correlate the unique  $\nu_s(OCO)$  to the specific  $\nu_o(OCO)$  normalized peak height analysis is employed.

Fig. 4 depicts the temperature dependent relative peak heights associated with the asymmetric stretching bands at 1543 cm<sup>-1</sup>, 1558 cm<sup>-1</sup>, and 1585 cm<sup>-1</sup> representing bdt-benzoate (44), bdt-benzoate (43), and bdt-benzoate (33), respectively, and compares them with the  $v_s(OCO)$  bdt-benzoate features at 1378 cm<sup>-1</sup>, 1373 cm<sup>-1</sup>, and 1353 cm<sup>-1</sup> in the DRIFTS spectra presented in Fig. 3. From the trends in intensity change as a function of temperature presented in Fig. 4, the oxidation state specific  $v_s(OCO)$  bands are identified through pairing with their  $v_a(OCO)$  counterparts.

In Fig. 4, as the temperature of ceria is increased from 25 to 100 °C no changes in any bdt-benzoate features are seen. At 200 °C the bands at 1543 cm<sup>-1</sup>, 1558 cm<sup>-1</sup>, 1373 cm<sup>-1</sup>, and 1353 cm<sup>-1</sup> increase, however, the bdt-benzoate bands at 1585 cm<sup>-1</sup>, associated with bdt-benzoate (33), and 1378 cm<sup>-1</sup> remain unchanged indicating that the  $\nu_s(\text{OCO})$  band at 1378 cm<sup>-1</sup> is also correlated to bdt-benzoate (33). From 300 to 450 °C all bdt-benzoate features increase. At 500 °C the bands at 1558 cm<sup>-1</sup>, 1585 cm<sup>-1</sup>, 1378 cm<sup>-1</sup>, and 1373 cm<sup>-1</sup> reach maximum intensity while the bands at 1543 cm<sup>-1</sup>, associated with bdt-benzoate (44), and 1353 cm<sup>-1</sup> have decreased in intensity indicating that the  $\nu_s(\text{OCO})$  band at 1353 cm<sup>-1</sup> represents bdt-benzoate (44) as well. The decrease in the  $\nu_a(\text{OCO})$  and  $\nu_s(\text{OCO})$  features of bdt-benzoate (44) is caused by the reduction of ceria surface metal sites from Ce<sup>4+</sup> to Ce<sup>3+</sup> that occurs at higher temperatures. By process of elimination the 1558 cm<sup>-1</sup> and 1373

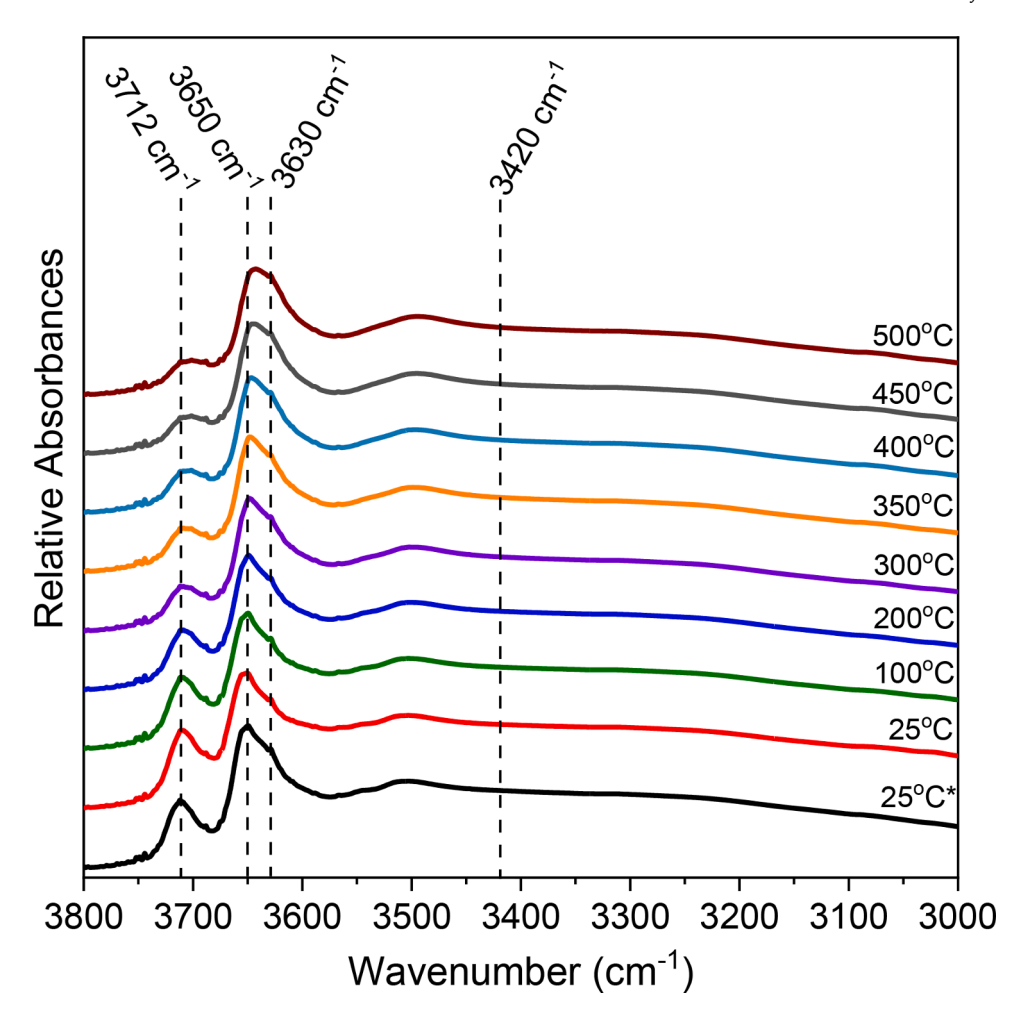


Fig. 6. Absolute DRIFTS of OH stretching region of the ceria surface before (25 °C\*), and after (25 °C) initial toluene adsorption and as a function of temperature.

cm<sup>-1</sup> bands are both determined to represent the  $\nu_{\alpha}(\text{OCO})$  and  $\nu_{s}(\text{OCO})$  of bdt-benzoate (43), respectively. In addition to identifying the oxidation state dependent  $\nu_{s}(\text{OCO})$  IR bands of bdt-benzoate, relative peak height analysis allows for cataloging mechanistic steps taking place on the catalytic surface.

Further utilizing relative peak height analysis of the spectra presented in Fig. 3 focusing on the transformation of benzyloxy, benzoate, and carbonate features allows for the elucidation of the mechanism for the oxidation of toluene to benzoate on the surface of ceria. Fig. 5 displays the relative peak height analysis of the DRIFTS spectra in Fig. 3 in order to better catalog the subtle band changes as a function of temperature. Fig. 5 depicts the temperature dependent relative peak heights associated with features representing the  $\nu$ (CO) of m-benzyloxy at 1095 cm<sup>-1</sup> and  $\nu$ (CO) of b-benzyloxy at 1040 cm<sup>-1</sup> and compares them with the  $\nu$ <sub>a</sub>(OCO) benzoate features at 1585 cm<sup>-1</sup>, 1558 cm<sup>-1</sup>, and1543 cm<sup>-1</sup> as well as the carbonate feature at 1440 cm<sup>-1</sup>. The  $\nu$ <sub>s</sub>(OCO) of benzoate species are omitted from this peak height analysis for brevity, as they follow an identical trend to their respective  $\nu$ <sub>a</sub>(OCO) counterpart.

In Fig. 5, as the temperature of the substrate is increased from 25 to 100 °C a decrease in the intensity of the m-benzyloxy features is observed while the b-benzyloxy increases in intensity with no change to the benzoate features indicating that m-benzyloxy is solely converting into b-benzyloxy. At 200 °C the intensity of two of the  $\nu_a(\text{OCO})$  bdt-benzoate features at 1558 cm $^{-1}$  (43) and 1543 cm $^{-1}$  (44) as well as the carbonate feature at 1440 begin to increase. The formation of carbonate is likely due to the separation of the benzene ring from the carbon of the chemisorbed carboxylate functional group of benzoate. Said carboxylate carbon then reacts with oxygen released from the substrate

as signified by the increase in the bdt-benzoate (43) feature indicating substrate reduction, or through interaction with physisorbed water or nearby surface OH species [28]. At 300 °C, b-benzyloxy features decrease, signifying its transformation into bdt-benzoate made apparent by the increase of the bands at  $1585 \text{ cm}^{-1}$ ,  $1558 \text{ cm}^{-1}$ , and  $1543 \text{ cm}^{-1}$ . The decrease in b-benzyloxy features and increases in all three bdt-benzoate features continue until 450 °C. At 500 °C bdt-benzoate (44) features decrease in intensity while b-benzyloxy continues to decrease, however, bdt-benzoate (43) and (33) features continue to increase in intensity. The increase in bdt-benzoate (43) and (33) occurs at a rate that outpaces the decrease in bdt-benzoate (44) indicating further transformation of b-benzyloxy into bdt-benzoate species. With the reduction of the surface being more wide spread at 500 °C the formed bdt-benzoate species are bound to (43) or (33) cerium sites [20,22,37, 46]. At 450 °C m-benzyloxy features cease to decrease in intensity and remain at the same intensity to 500 °C while the b-benzyloxy features continue to decrease indicating that at temperatures above 400 °C the production of benzoate is dependent on b-benzyloxy species only. The lack of an increase in benzoate feature intensity and a decrease in m-benzyloxy feature intensity between 25 and 100 °C indicates that the transformation of m-benzyloxy is not leading to the production of benzoate species. Additionally, the increase of benzoate feature intensity and the stagnant m-benzyloxy feature from 450 to 500 °C indicates that the formation of benzoate species at temperatures optimal for complete surface reduction is independent of the m-benzyloxy species.

From the DRIFTS spectra and subsequent peak height analysis presented in Fig. 3 and Fig. 5 respectively, it is clear that toluene binds to the surface as the two distinct benzyloxy species, m-benzyloxy and b-

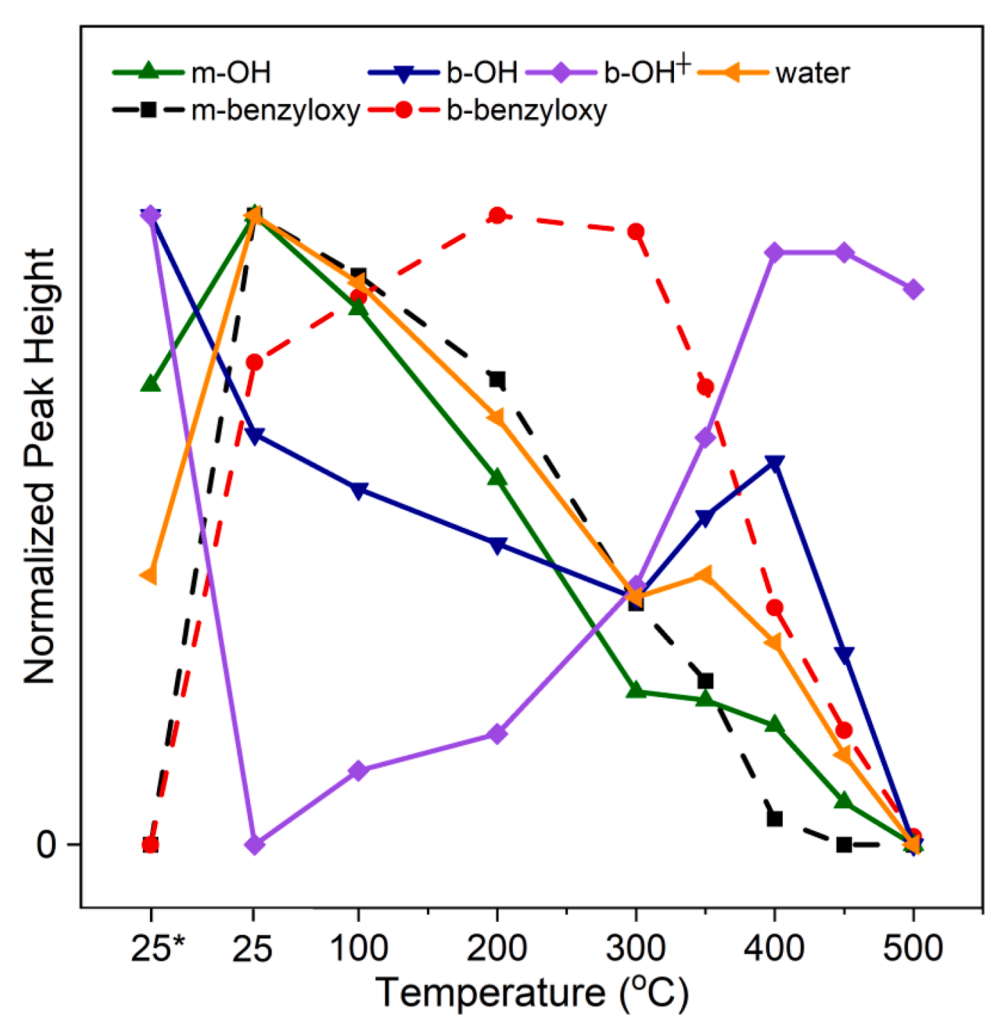


Fig. 7. Temperature dependent normalized peak height analysis of OH (–) and benzyloxy (- -) features. m-OH (3712 cm<sup>-1</sup>), b-OH (3650 cm<sup>-1</sup>), b-OH<sup>†</sup> (3630 cm<sup>-1</sup>), water (3420 cm<sup>-1</sup>), m-benzyloxy (1095 cm<sup>-1</sup>), b-benzyloxy (1040 cm<sup>-1</sup>). +-vacancy adjacent.

benzyloxy. m-benzyloxy is transformed into b-benzyloxy upon heating the system from 25 °C to 200 °C followed by the transformation of b-benzyloxy into bdt-benzoate species at temperatures ranging from 200 °C to 500 °C. In order to completely characterize the mechanism for the oxidation of toluene to bdt-benzoate on the surface of ceria, the sources of oxygen and their role in the transformation of toluene to benzyloxy to benzoate needs to be understood.

# 3.1.2. Hydroxyl role DRIFTS characterization

Cataloging surface hydroxyl activity during catalysis is vital for fully discerning the mechanism. Surface hydroxyls are responsible for aiding in binding adsorbates as well as acting as sources of oxygen and/or hydrogen [31,33,37,52-56]. Changes in the IR intensity of hydroxyl features indicate that OH species are active in the reaction. A decrease in a unique OH feature stipulates that particular OH species is transforming during the reaction. Fig. 6 depicts the absolute DRIFTS spectra, obtained using a gold foil background, of the hydroxyl stretching region (3800–3000 cm<sup>-1</sup>) of ceria upon exposure to toluene as a function of temperature. Post toluene introduction, the subsequent heating of the system results in changes to four distinct OH bands: m-OH features at 3712 cm<sup>-1</sup>, b-OH features with no adjacent oxygen vacancies (b-OH) at  $3650~\text{cm}^{-1}$ , b-OH features with adjacent oxygen vacancies (b-OH $^{\dagger}$ ) at  $3630\,\mathrm{cm}^{-1}$ , and physisorbed water on the surface of ceria represented by the broad feature centered at 3420 cm<sup>-1</sup> [32,37,57-59]. The broad band centered at 3510 cm<sup>-1</sup> is associated with interstitial oxyhydroxide species and triply bound OH groups [32,37,57,58,60]. The lack of meaningful change in the intensity of the  $3510~\rm cm^{-1}$  band signifies the inactivity of the associated species throughout the oxidation of toluene, thus, this band is more likely associated with interstitial oxyhydroxide species.

From the DRIFTS spectra in Fig. 6, the changes in hydroxyl features, before (25 °C\*) and (25 °C) after the introduction of toluene and as the surface temperature increases, are subtle. Peak height analysis is employed to perceive the transformation of hydroxyl features during the initial binding and oxidation of toluene on the surface of ceria. By simultaneously monitoring the transformation of OH features in relation to benzyloxy features with relative peak height analysis, a clear understanding of hydroxyl activity during the transformation of m-benzyloxy to b-benzyloxy is achieved. Fig. 7 compares the relative peak height of surface OH features, namely m-OH at 3712 cm $^{-1}$ , b-OH at 3650 cm $^{-1}$ , b-OH $^{\dagger}$  at 3630 cm $^{-1}$ , and physisorbed water at 3420 cm $^{-1}$ , with m-benzyloxy at 1095 cm $^{-1}$  and b-benzyloxy at 1040 cm $^{-1}$  to determine their correlation throughout the study.

In Fig. 7, after toluene is introduced (25 °C\* to 25 °C) there is a drastic increase in m-benzyloxy and b-benzyloxy features at 1095 cm $^{-1}$  and 1040 cm $^{-1}$  respectively while there is a decrease in both b-OH and b-OH $^{+}$  features yet an increase in m-OH and physisorbed water features. The decrease in b-OH and b-OH $^{+}$  features as both benzyloxy features increase indicates that the b-OH and b-OH $^{+}$  play a role in the chemisorption of toluene; however, chemisorption does not account for the increase in m-OH species. The surface of ceria is populated with both hydroxyl species and surface lattice oxygen, the increase in m-OH

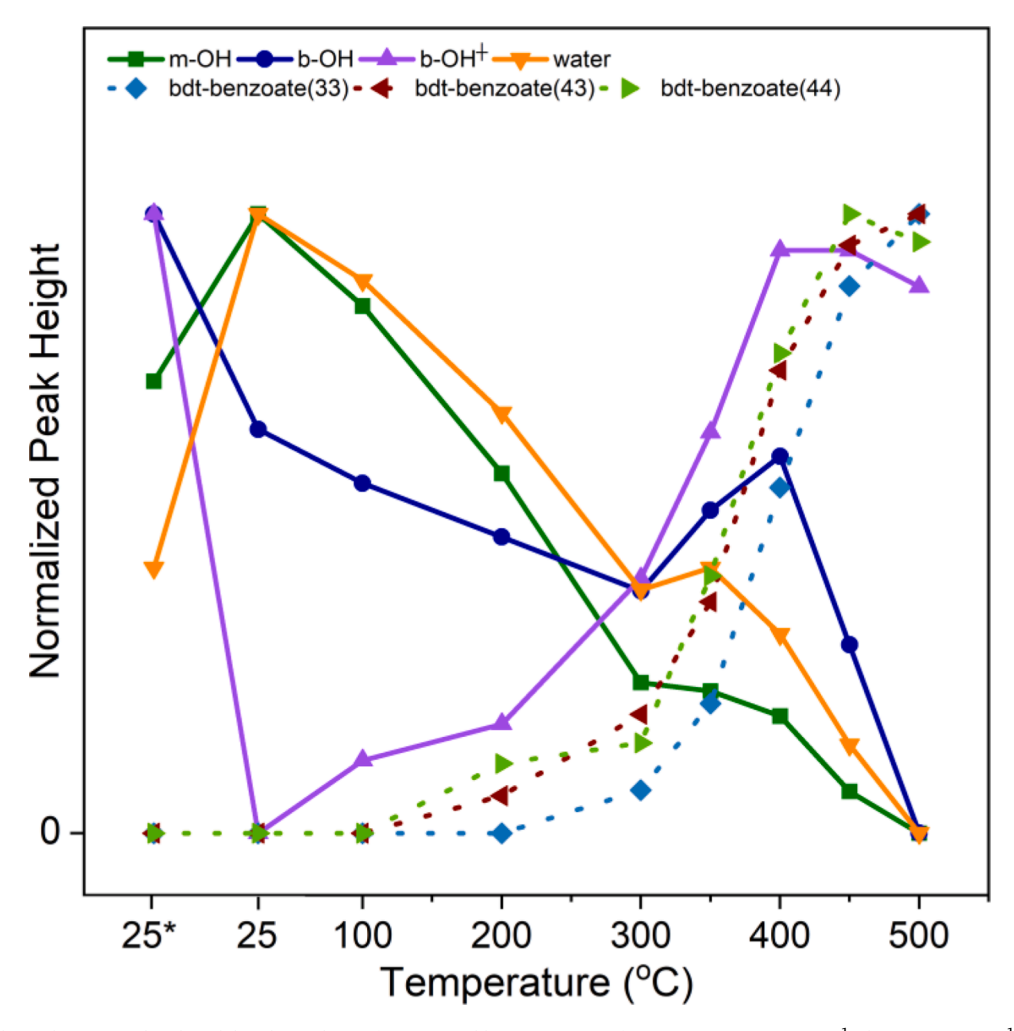


Fig. 8. Temperature dependent normalized peak height analysis of OH (–) and benzoate (••••) features. m-OH (3712 cm<sup>-1</sup>), b-OH (3650 cm<sup>-1</sup>), b-OH<sup>+</sup> (3630 cm<sup>-1</sup>), and water (3420 cm<sup>-1</sup>), bdt-benzoate (33) (1585 cm<sup>-1</sup>), bdt-benzoate (43) (1558 cm<sup>-1</sup>), bdt-benzoate (44) (1543 cm<sup>-1</sup>). +vacancy adjacent.

species indicates that toluene is also interacting with surface oxygen resulting in the release of a hydrogen that is free to form an OH group after interacting with an additional nearby surface oxygen [32,37,57, 61–63]. As the temperature is increased from 25 to 200 °C there are decreases in the intensities of the 3712 cm<sup>-1</sup> (m-OH) and 3650 cm<sup>-1</sup> (b-OH) surface hydroxyl species as well as 3400 cm<sup>-1</sup> (physisorbed water) yet an increase in 3630 cm<sup>-1</sup> (b-OH<sup>+</sup>) feature all while the m-benzyloxy peak, at  $1095~\text{cm}^{-1}$ , decreases and b-benzyloxy feature, at 1040 cm<sup>-1</sup>, increases in intensity. The only source for continued b-benzyloxy production is the reaction of m-benzyloxy with an adjacent oxygen species. The decrease in m-OH and b-OH species as m-benzyloxy decreases and b-benzyloxy increases indicates that m-benzyloxy is interacting with either a m-OH or b-OH species to form b-benzyloxy. If m-benzyloxy interacts with an m-OH species, the hydroxyl would shift to an adjacent Ce site forming a b-OH species. If m-benzyloxy interacts with a b-OH species the b-OH could transform into a m-OH with the OH shifting from being connected to two cerium centers to being attached to a single cerium center.

Fig. 7 also indicates that as the temperature of the substrate is increased beyond 300 °C, there is an increase in intensity of b-OH and b-OH $^+$  species, and beyond 400 °C, m-OH, b-OH, and water all decrease in intensity. In order to properly characterize the changes in hydroxyl features at temperatures above 300 °C it is necessary to compare the evolution of benzoate species on the surface with changes in the surface hydroxyl species in question. The peak height analysis of bdt-benzoate (44), bdt-benzoate (43), bdt-benzoate (33), m-OH, b-OH, b-OH  $^+$ , and water is presented in Fig. 8 from 25 to 500 °C where m-OH and b-OH

species are seen facilitating the production of bdt-benzoate species through interaction with b-benzyloxy. The discussion of Fig. 8 will be centered on temperatures from 300 to 500  $^{\circ}$ C as this is this is the temperature range where a drastic increase in benzoate species occurs and the analysis of the changing hydroxyl features at temperatures below 300  $^{\circ}$ C was carried out in the discussion of Fig. 7.

Fig. 8 shows that with the increase of bdt-benzoate species on the surface from 300 to 500 °C there is further evolution of surface hydroxyls and water. The decrease in intensity of m-OH at temperatures from 300 to 500 °C and b-OH features from 400 to 500 °C is a result of these hydroxyls acting as sources of oxygen for benzyloxy to benzoate transformation, however the slow decrease of m-OH features and increase of b-OH features from 350 to 400 °C is likely caused by the release of hydrogen from benzyloxy to benzoate transformation. As benzyloxy is transformed into benzoate, hydrogen is released and free to interact with oxygen on the surface of CeO<sub>2</sub> [20,21,35,37,64-66]. The released hydrogen interacting with surface oxygen produces surface OH species or water, as indicated by an increase in b-OH features at temperatures from 350 to 400  $^{\circ}\text{C}$  and water features at 300  $^{\circ}\text{C}$ . The anomaly of the continued increase in b-OH<sup>+</sup> from 25 to 400 °C is likely caused by the reduction of the ceria surface resulting in oxygen vacancies forming adjacent to already formed b-OH features.

From Fig. 7 it is apparent that b-OH and b-OH<sup>†</sup> species are capable of facilitating the chemisorption of toluene but a concrete investigation on why m-OH species are seen increasing after toluene introduction at 25 °C is needed. To add finer detail to the role hydroxyls play in the chemisorption of toluene, difference DRIFTS spectra are utilized to

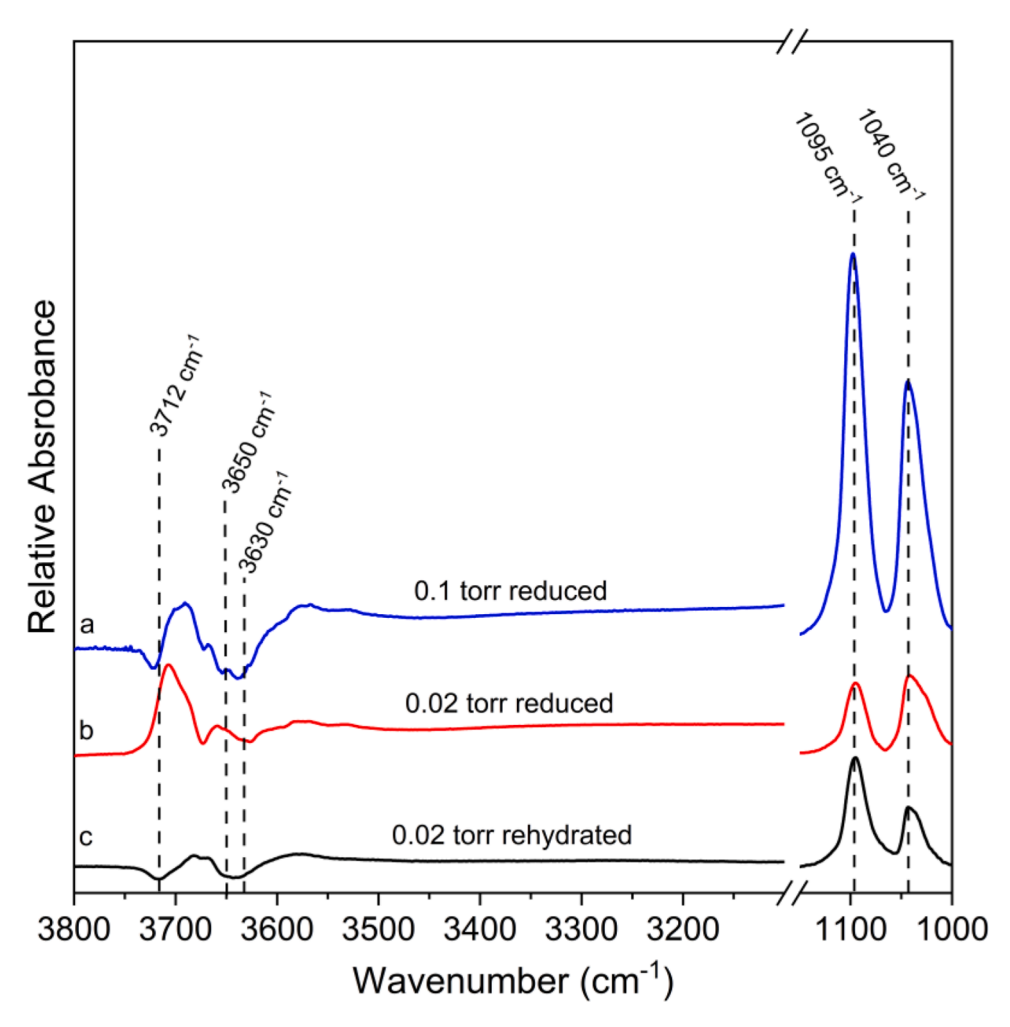


Fig. 9. Difference DRIFTS of OH stretching and alkoxy carbon-oxygen stretching region of (a) reduced ceria after 0.1 torr of toluene introduction at 25 °C, (b) reduced ceria after 0.02 torr of toluene introduction at 25 °C, (c) rehydrated ceria after 0.02 torr toluene introduction at 25 °C.

compare the changes in OH and benzyloxy features on the surface of CeO<sub>2</sub> after toluene is introduced under three unique conditions and is depicted in Fig. 9. Spectra (a) and (b) in Fig. 9 represents the difference DRIFTS spectra of heat-treated CeO2 cooled to 25 °C after the introduction of either 0.1 torr (a) or 0.02 torr (b) toluene, using the cooled to 25 °C CeO<sub>2</sub> as the background. The partial adsorbate coverage shown in spectrum (b) elucidates which surface species react first when a limited amount of adsorbate is available. To further clarify the role of hydroxyls. the heat-treated ceria is cooled to 25 °C and rehydroxylated by introducing 0.5 torr of water vapor for 30 min. The rehydroxylated substrate is evacuated overnight and a spectrum is taken which is then used as a background to clearly show changes to this substrate when exposed to 0.02 torr of toluene; the resulting difference DRIFTS spectrum is labeled (c) in Fig. 9. By introducing water to the cooled substrate, the maximum amount of surface OH species are formed by water reacting with the surface resulting in OH species available to fill oxygen vacancies and H available to interact with surface lattice oxygen forming OH species. Thus spectrum (c) in Fig. 9 elucidates which surface species react first when a limited amount of adsorbate is available and maximum OH species are available.

From the toluene saturated surface (spectrum (a) in Fig. 9) the hydroxyl activity is not immediately obvious. After toluene introduction, an increase of m-OH features and decrease in b-OH features occurs. A hydroxyl species binding toluene and transforming it into benzyloxy would result in a decrease in the respective OH IR feature. In spectrum (a) b-OH features decrease and m-OH features increase. The negative feature in spectrum (a) at  $3712~{\rm cm}^{-1}$  is caused by the red shift of m-OH

species through hydrogen bonding with now adjacent benzyloxy groups. Observing the changes in hydroxyl features after partially covering the surface with toluene (spectrum (b) in Fig. 9) leads to a better understanding of the production of m-OH species on the surface of ceria. Here, as benzyloxy forms on the surface, all hydroxyl features increase signifying that benzyloxy species are forming through the interaction with surface lattice oxygen. As toluene chemisorbs to the surface the terminal methyl group of toluene loses a hydrogen. The released hydrogen is available to interact with a surface oxygen producing m-OH and b-OH species. This indicates that the increase in m-OH (3712 cm<sup>-1</sup>) features in spectrum (a) was caused by the interaction of toluene with surface oxygen components resulting in the release of hydrogen now free to react with the ceria surface. In order to more confidently state that, in spectrum (a), b-OH (3650 cm<sup>-1</sup>) species are additionally responsible for binding toluene the partial coverage study was repeated with a rehydrated ceria surface (spectrum c). In spectrum (c) a decrease in m-OH (3712 cm<sup>-1</sup>) feature is observed but an increase in an adjacent peak indicates that this is, again, a peak shift as surface m-OH hydrogen bond with adjacent benzyloxy species. There is a decrease of b-OH features at 3650 cm<sup>-1</sup> indicating that b-OH species are a source of oxygen for toluene chemisorption. To sum up, toluene can interact with either surface lattice oxygen or b-OH forming either m-benzyloxy or b-benzyloxy species. With the need for b-OH species and surface lattice oxygen to facilitate the chemisorption of toluene, the CeO<sub>2</sub> (100) and (110) faces are most likely the surfaces at which the observed toluene oxidation occurs as these planes contain reactive b-OH and surface lattice oxygen species [32,56,67,68].

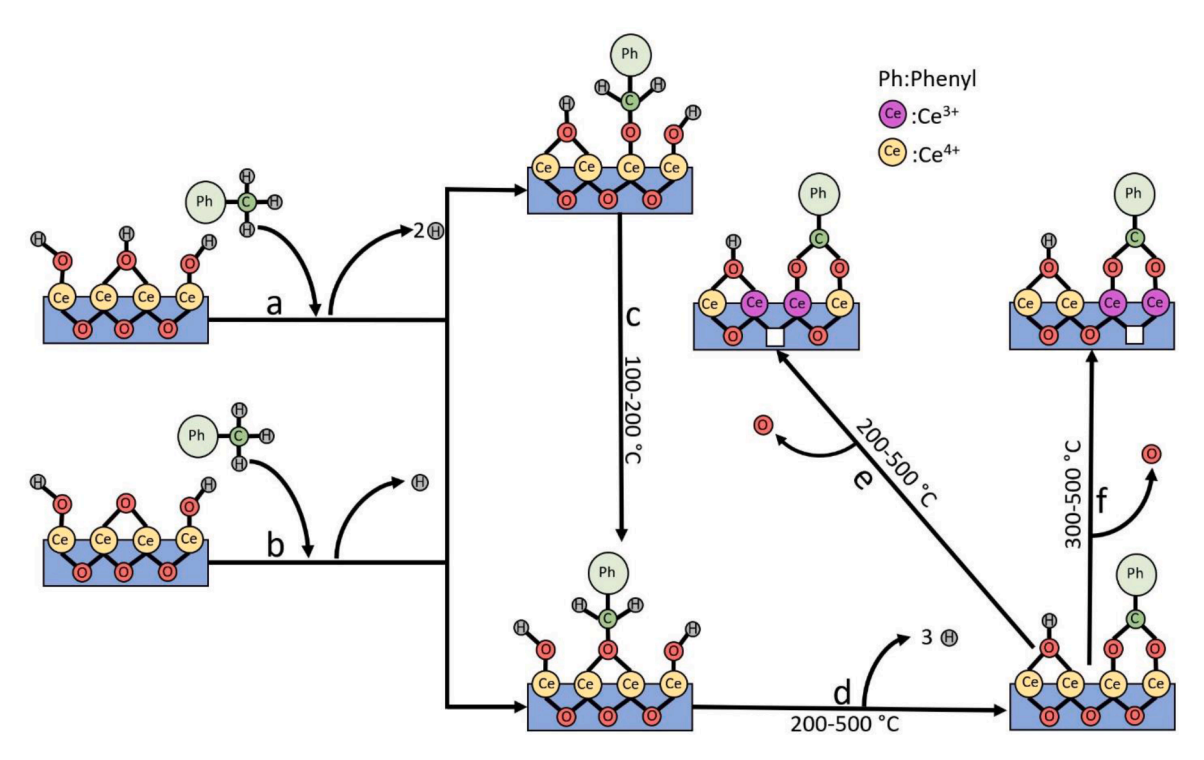
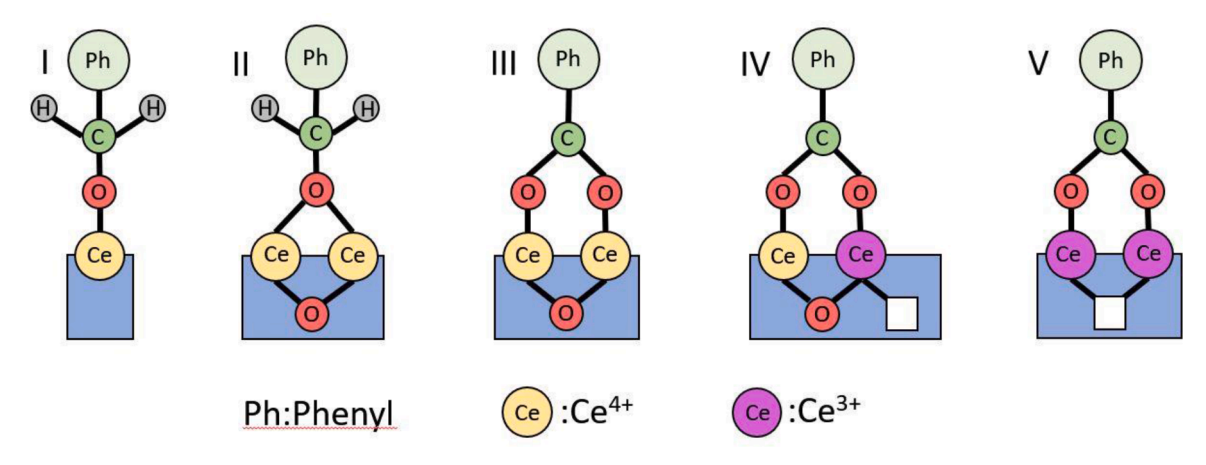


Fig. 10. Mechanism for the oxidation of toluene to bdt-benzoate on the surface of ceria.



Scheme 1. Structures of benzyloxy and benzoate species. (I) m-benzyloxy, (II) b-benzyloxy, (III) bdt-benzoate (44), (IV) bdt-benzoate (43), (V) bdt-benzoate (33).

### 3.2. Reaction mechanism

To date, there have been a few attempts to describe the mechanism for the oxidation of toluene on the surface of ceria. Toluene has been proposed to initially bind to the catalytic surface of ceria through its terminal methyl group followed by transformation into benzaldehyde and finally benzoate [11,28]. With the evidence provided from these DRIFTS experiments, a new mechanistic pathway for the conversion of toluene to benzoate on ceria is revealed that incorporates benzyloxy as an intermediate species. From the information discerned from the DRIFTS and subsequent peak height analysis presented in Figs. 3 and 5–9, a comprehensive mechanism for the chemisorption of toluene and conversion into bdt-benzoate is determined and is illustrated in Fig. 10.

Fig. 10 details the mechanism for the chemisorption of toluene and subsequent conversion to bdt-benzoate. Both m-benzyloxy and b-benzyloxy are produced when toluene interacts with either surface b-OH species or surface oxygen species on ceria at room temperature (paths a and b in Fig. 10). The binding pathways are supported by the decrease in

b-OH features after toluene introduction observed in spectra (a) and (c) in Fig. 9 and the increase in all hydroxyl species after toluene introduction observed in spectrum (b) in Fig. 9. As the substrate is heated from 25 to 200  $^{\circ}$ C, m-benzyloxy reacts with an adjacent m-OH or b-OH (path c in Fig. 10) to form a b-benzyloxy group. The transformation of m-benzyloxy to b-benzyloxy through OH interaction is supported by the continued loss of m-OH and b-OH species as m-benzyloxy features decrease and b-benzyloxy features increase as depicted in Fig. 7.

The oxidation of b-benzyloxy to bdt-benzoate (43) and bdt-benzoate (33) depicted in Fig. 10 is initiated through the oxidation of b-benzyloxy to bdt-benzoate (44) (path d). As the system reaches 200 °C the carbon in b-benzyloxy interacts with cerium bound oxygen found in an adjacent OH species resulting in its transformation into bdt-benzoate (44). Transformation of b-benzyloxy and adjacent hydroxyl species is supported by the dependence of bdt-benzoate formation on b-benzyloxy species at 450 to 500 °C as seen in Fig. 5 and the decrease in m-OH and b-OH features that occurs until 300 °C is reached and the steady decrease of m-OH features at temperatures above 300 °C as seen in Figs. 7 and 8.

The production of bdt-benzoate (44) from the oxidation of b-benzyloxy continues up to 500 °C supported by the continued decrease in b-benzyloxy features up to 500 °C seen in Fig. 5. At 200 °C bdt-benzoate (43) features are also seen forming in Fig. 3 as minute amounts of oxygen begin to leave the surface of the substrate (path e). The transformation of b-benzyloxy also results in the conversion of m-OH to b-OH in an attempt to keep all cerium atoms satisfied. The transformation of m-OH to b-OH is indicated by the increase in b-OH features seen in Fig. 8 at 300  $^{\circ}\text{C}$  that occurs in tandem with the drastic increase in benzoate production. The transformation of m-OH to b-OH is likely occurring at 200 °C, when benzoate production initially begins, but the production of benzoate at this temperature is minimal and is likely offset by the continued transformation of m-benzyloxy to b-benzyloxy. At 300 °C bdtbenzoate (33) is observed as ceria continues to be reduced and is supported by the growth of its IR features detailed in Fig. 3 (path f). The departure of oxygen from the surface at temperatures > 200 °C is enabled through two paths. The first is through the natural reduction of CeO<sub>2</sub> as the substrate temperature increases towards 500 °C as indicated by the increase in bdt-benzoate (33) and (43) in Figs. 4, 5, and 8. The second is through the released hydrogen, from toluene oxidation, interacting with surface lattice oxygen and forming new hydroxyls followed by water from further hydrogen interaction which then desorbs resulting in an oxygen vacancy [67,68].

In Fig. 5, at 500  $^{\circ}$ C, the reduction of the surface becomes more widespread resulting in higher transformation levels of bdt-benzoate (44) to bdt-benzoate (43) and bdt-benzoate (33) (paths e and f in Fig. 10). The increased conversion of bdt-benzoate (44) to bdt-benzoate (43) and bdt-benzoate (33) is supported by the decrease in bdt-benzoate (44) features and increase in bdt-benzoate (43) and bdt-benzoate (33) seen at 500  $^{\circ}$ C in Fig. 5.

#### 4. Conclusion

The reaction of toluene with ceria nanoparticles was investigated via  $in\ situ\ DRIFTS$ . DRIFTS spectra and subsequent peak height analysis as a function of temperature were interpreted to characterize the symmetric  $\nu(OCO)$  of benzoate species and determine the mechanism of toluene oxidation on the surface of ceria. Toluene reacts with the ceria surface to produce m-benzyloxy and b-benzyloxy groups on ceria. The m-benzyloxy species are converted to b-benzyloxy through interaction with an adjacent surface hydroxyl. The b-benzyloxy is then transformed into benzoate. No evidence of benzaldehyde was observed on the surface.

Additionally, the interpretation of DRIFTS spectra and peak height analysis as a function of temperature allowed for the determination of the role surface hydroxyls play in the initial binding and oxidation of toluene on the ceria surface. When toluene interacts with a b-OH species or surface lattice oxygen both m-benzyloxy and b-benzyloxy can be formed while m-OH species do not play an active role in binding. Once 200  $^{\circ}\text{C}$  is reached b-benzyloxy interacts with an adjacent hydroxyl forming bdt-benzoate. At temperatures above 300  $^{\circ}\text{C}$ , the reduction of the ceria surface becomes more widespread and there is an increased conversion of bdt-benzoate (44) to bdt-benzoate (43) and bdt-benzoate (33). From 450 to 500  $^{\circ}\text{C}$  all m-benzyloxy species have been transformed into b-benzyloxy which continues to solely transform into bdt-benzoate species.

From this study a comprehensive mechanism for the oxidation of toluene on the surface of ceria is realized. b-benzyloxy is found to be the direct precursor to benzoate and is the only available intermediate species observed transforming into bdt-benzoate species at 450–500 °C, the optimal catalytic temperatures for ceria. Benzaldehyde, a previously proposed intermediate species was not observed, indicating it is not a necessary species in the oxidation of toluene on the surface of ceria. Knowledge of the importance of b-benzyloxy species will enable optimization of oxidation on the surface of ceria through reaction condition control. The characterization of the roles of OH and surface oxygen species play in the binding and transformation of toluene to benzoate on

the surface of ceria solidifies the importance of OH species during the oxidation of toluene. Toluene's transformation and oxidation into benzoate, facilitated by surface OH species and surface oxygens, is an essential process during the catalytic combustion of toluene. The temperature dependent intermediate and hydroxyl species activity information presented here will help to better optimize the catalytic combustion of toluene through heat cycle regulation to promote the b-benzyloxy intermediate species and selecting ceria morphologies that have surfaces predominantly inhabited by b-OH and surface lattice oxygens. The toluene transformation process on the surface of ceria has now been well documented, considerably advancing the understanding of the catalytic combustion of toluene mechanism.

# CRediT authorship contribution statement

Paul K. Huttunen: Conceptualization, Methodology, Validation, Formal analysis, Investigation, Resources, Writing – original draft, Visualization, Project administration. Daniela Labadini: Formal analysis, Investigation, Writing – review & editing. Genevieve Asselin: Formal analysis, Investigation. Sabrina S. Hafiz: Writing – review & editing. Sumeyra Gokalp: Writing – review & editing. Maria D. Kipreos: Writing – review & editing. Michelle Foster: Methodology, Writing – review & editing, Visualization, Supervision, Project administration, Funding acquisition.

### **Declaration of Competing Interest**

The authors declare that they have no known competing financial interests or personal relationships that could have appeared to influence the work reported in this paper.

# Acknowledgments

The authors would like to thank Dr. Shao-Liang Zheng, the Director of the X-ray Laboratory in the Department of Chemistry and Chemical Biology at Harvard University, for assistance with collecting the PXRD spectra of our  $CeO_2$  nanoparticles.

## Supplementary materials

Supplementary material associated with this article can be found, in the online version, at doi:10.1016/j.susc.2022.122042.

### References

- [1] B. Chen, B. Wang, Y. Sun, X. Wang, M. Fu, J. Wu, L. Chen, Y. Tan, D. Ye, Plasmaassisted surface interactions of Pt/CeO<sub>2</sub> catalyst for enhanced toluene catalytic oxidation, Catalysts. 9 (2018) 1–18, https://doi.org/10.3390/catal9010002.
- [2] J.M. Donald, K. Hooper, C. Hopenhayn-rich, J.M. Donald, K. Hooper, Reproductive and developmental toxicity of toluene: a review, Environ. Health Perspect. 94 (1991) 237–244.
- [3] A. Manuscript, Review of toluene action: clinical evidence, animal studies and molecular targets, J. Drug Alcohol Res. 3 (2014) 1–15, https://doi.org/10.4303/ jdar/235840.Review.
- [4] J. Niu, H. Qian, J. Liu, H. Liu, P. Zhang, E. Duan, Process and mechanism of toluene oxidation using Cu<sub>1-y</sub>Mn<sub>2</sub>Ce<sub>y</sub>O<sub>x</sub>/sepiolite prepared by the co-precipitation method, J. Hazard. Mater. 357 (2018) 332–340, https://doi.org/10.1016/j. ihazmat.2018.06.004.
- [5] Z. Jiang, C. Chen, M. Ma, Z. Guo, Y. Yu, C. He, Rare-earth element doping-promoted toluene low-temperature combustion over mesostructured CuMCeO<sub>x</sub> (M = Y, Eu, Ho, and Sm) catalysts: the indispensable role of *in situ* generated oxygen vacancies, Catal. Sci. Technol. 8 (2018) 5933–5942, https://doi.org/10.1039/c8cv01849a.
- [6] J.J. Spivey, Complete catalytic oxidation of volatile organicst, Ind. Eng. Chem. Res. 26 (1987) 2165–2180, https://doi.org/10.1021/ie00071a001.
- [7] S. Scirè, S. Minicò, C. Crisafulli, C. Satriano, A. Pistone, Catalytic combustion of volatile organic compounds on gold /cerium oxide catalysts, 2003.
- [8] K. Inoue, S. Somekawa, Treatment of Volatile Organic Compounds with a Pt/ Co<sub>3</sub>O<sub>4</sub>-CeO<sub>2</sub> Catalyst, Chem. Eng. Technol. 42 (2019) 257–260, https://doi.org/ 10.1002/ceat.201800245.

- [9] Q. Wang, K. Yeung, M.A. Bañares, Ceria and its related materials for VOC catalytic combustion: a review, Catal. Today 356 (2020) 141–154, https://doi.org/10.1016/ i.cattod.2019.05.016.
- [10] Q. Wang, Y. Li, A. Serrano-Lotina, W. Han, R. Portela, R. Wang, M.A. Bañares, K. L. Yeung, Operando investigation of toluene oxidation over 1D Pt/CeO<sub>2</sub> derived from Pt cluster-containing MOF, J. Am. Chem. Soc. 143 (2021) 196–205, https://doi.org/10.1021/jacs.0c.08640
- [11] X. Chen, X. Chen, E. Yu, S. Cai, H. Jia, J. Chen, P. Liang, *In situ* pyrolysis of Ce-MOF to prepare CeO<sub>2</sub> catalyst with obviously improved catalytic performance for toluene combustion, Chem. Eng. J. 344 (2018) 469–479, https://doi.org/10.1016/i.cei.2018.03.091.
- [12] B. Zhao, Y. Jian, Z. Jiang, R. Albilali, C. He, Revealing the unexpected promotion effect of EuO<sub>x</sub> on Pt/CeO<sub>2</sub> catalysts for catalytic combustion of toluene, Chin. J. Catal. 40 (2019) 543–552, https://doi.org/10.1016/S1872-2067(19)63292-4.
- [13] A. Aboukaïs, M. Skaf, S. Hany, R. Cousin, S. Aouad, A comparative study of Cu, Ag and Au doped CeO<sub>2</sub> in the total oxidation of volatile organic compounds (VOCs), Mater. Chem. Phys. 177 (2016) 570–576, https://doi.org/10.1016/j.matchemphys.2016.04.072.
- [14] E.M. Cordi, J.L. Falconer, Oxidation of volatile organic compounds on Al<sub>2</sub>O<sub>3</sub>, Pd/Al<sub>2</sub>O<sub>3</sub>, and PdO/Al<sub>2</sub>O<sub>3</sub> catalysts, J. Catal. 162 (1996) 104–117.
- [15] H. Yi, X. Xie, X. Tang, S. Zhao, K. Yang, Demonstration of Low-Temperature Toluene Degradation Mechanism on Hydrotalcite-Derived Oxides with Ultrasonic Intervention, Elsevier, 2019, https://doi.org/10.1016/j.cej.2019.05.190.
- [16] J. Niu, H. Qian, J. Liu, H. Liu, P. Zhang, E. Duan, Process and Mechanism of Toluene Oxidation Using Cu<sub>1-y</sub>Mn<sub>2</sub>Ce<sub>y</sub>O<sub>x</sub>/sepiolite Prepared By the Co-Precipitation Method, Elsevier, 2018, https://doi.org/10.1016/j. ihazmat.2018.06.004.
- [17] S. Ordóñez, L. Bello, H. Sastre, R. Rosal, V.D. Fernando, Kinetics of the deep oxidation of benzene, toluene, n-hexane and their binary mixtures over a platinum on γ-alumina catalyst, 2002.
- [18] C. Doornkamp, V. Ponec, The universal character of the Mars and Van Krevelen mechanism, J. Mol. Catal. A Chem. 162 (2000) 19–32.
- [19] B. Liu, H. Wu, I.P. Parkin, Gaseous photocatalytic oxidation of formic acid over TiO<sub>2</sub>: a comparison between the charge carrier transfer and light-assisted mars – van Krevelen pathways, J. Phys. Chem. C 123 (2019) 22261–22272, https://doi. ore/10.1021/acs.ipcc.9b05357.
- [20] S. Rousseau, O. Marie, P. Bazin, M. Daturi, V. Harle, A.V. Cedex, Investigation of methanol oxidation over Au/catalysts using operando IR spectroscopy: determination of the active sites, intermediate/spectator species, and reaction mechanism, J. Am. Chem. Soc. 132 (2010) 10832–10841, https://doi.org/ 10.1021/ja1028809
- [21] G. Díaz, D.G. Araiza, A. Gómez-cortés, G. Díaz, Reactivity of methanol over copper supported on well-shaped CeO<sub>2</sub>: a TPD-DRIFTS study, Catal. Sci. Technol. 7 (2017) 5224–5235, https://doi.org/10.1039/c7cy00984d.
- [22] T. Cao, R. You, X. Zhang, S. Chen, D. Li, Z. Zhang, W. Huang, An in situ DRIFTS mechanistic study of CeO<sub>2</sub>-catalyzed acetylene semihydrogenation reaction, Phys. Chem. Chem. Phys. 20 (2018) 9659–9670, https://doi.org/10.1039/c8cp00668g.
- [23] G. Jacobs, B.H. Davis, In situ DRIFTS investigation of the steam reforming of methanol over Pt/ceria, Appl. Catal. A Gen. 285 (2005) 43–49, https://doi.org/ 10.1016/j.apcata.2005.02.006.
- [24] N.M. Martin, F. Hemmingsson, A. Schaefer, M. Ek, L.R. Merte, U. Hejral, J. Gustafson, M. Skoglundh, Catalysis science & technology methanation over ceria supported Rh and Ni catalysts under atmospheric pressure conditions, Catal. Sci. Technol. 9 (2019) 1644–1653, https://doi.org/10.1039/c8cy02097c.
- [25] A.S. Malik, S.F. Zaman, A.A. Al-zahrani, M.A. Daous, H. Driss, L.A. Petrov, Development of highly selective PdZn/CeO<sub>2</sub> and Ca-doped PdZn/CeO<sub>2</sub> catalysts for methanol synthesis from CO<sub>2</sub> hydrogenation, Appl. Catal. A Gen. 560 (2018) 42–53, https://doi.org/10.1016/j.apcata.2018.04.036.
- [26] O.A. Ojelade, S.F. Zaman, M.A. Daous, A.A. Al-zahrani, A.S. Malik, H. Driss, G. Shterk, J. Gascon, Optimizing Pd: Zn molar ratio in PdZn/CeO<sub>2</sub> for CO<sub>2</sub> hydrogenation to methanol, Appl. Catal. A Gen. 584 (2019) 1–13, https://doi.org/ 10.1016/j.apcata.2019.117185.
- [27] O.A. Ojelade, S.F. Zaman, A review on Pd based catalysts for CO<sub>2</sub> hydrogenation to methanol: in-depth activity and DRIFTS mechanistic study, Catal. Surv. Asia 24 (2020) 11–37, https://doi.org/10.1007/s10563-019-09287-z.
- [28] L.C.D.Y. Qi Zhang, S. Mo, J. Li, Y. Sun, M. Zhang, P. Chen, M. Fu, J. Wu, In situ DRIFT spectroscopy insights into the reaction mechanism of CO and toluene cooxidation over Pt-based catalysts, Catal. Sci. Technol. 9 (2019) 4358–4551, https://doi.org/10.1039/c9cy00751b.
- [29] J. Li, H. Na, X. Zeng, T. Zhu, Z. Liu, In situ DRIFTS investigation for the oxidation of toluene by ozone over Mn /HZSM-5, Ag / HZSM-5 and Mn – Ag / HZSM-5 catalysts, Appl. Surf. Sci. 311 (2014) 690–696, https://doi.org/10.1016/j. apsusc.2014.05.138.
- [30] R. Li, L. Zhang, S. Zhu, S. Fu, X. Dong, S. Ida, L. Zhang, L. Guo, Applied catalysis a, general layered & MnO<sub>2</sub> as an active catalyst for toluene catalytic combustion, Appl. Catal. A Gen. 602 (2020), 117715, https://doi.org/10.1016/j.aocata.2020.117715.
- [31] Z. Liu, E. Huang, I. Orozco, W. Liao, R.M. Palomino, N. Rui, S. Nem, D.C. Grinter, M. Mahapatra, P. Liu, Water-promoted interfacial pathways in methane oxidation to methanol on a CeO<sub>2</sub>-Cu<sub>2</sub>O catalyst, Science 368 (2020) 513–517, https://doi. org/10.1126/science.pha5005
- [32] L. Luo, J.D. Lacoste, N.G. Khamidullina, E. Fox, D.D. Gang, R. Hernandez, H. Yan, Investigate interactions of water with mesoporous ceria using in situ VT-DRIFTS, Surf. Sci. 691 (2020), 121486, https://doi.org/10.1016/j.susc.2019.121486.

- [33] M.D. Kipreos, M. Foster, Water interactions on the surface of 50 nm rutile TiO<sub>2</sub> nanoparticles using in situ DRIFTS, Surf. Sci. 677 (2018) 1–7, https://doi.org/10.1016/j.susc.2018.05.005.
- [34] Y. Lykhach, V. Joha, H.A. Aleksandrov, S.M. Kozlov, M. Happel, P.S. Petkov, N. Tsud, G.N. Vayssilov, K.C. Prince, K.M. Neyman, J. Libuda, Water chemistry on model ceria and Pt/ceria catalysts, J. Phys. Chem. C 116 (2012) 12103–12113, https://doi.org/10.1021/jp302229x.
- [35] S. Zhao, S. Wang, Y. Zhao, X. Ma, An in situ infrared study of dimethyl carbonate synthesis from carbon dioxide and methanol over well-shaped CeO<sub>2</sub>, Chin. Chem. Lett. 28 (2017) 65–69, https://doi.org/10.1016/j.cclet.2016.06.003.
- [36] X. Wu, X. Gong, Clustering of oxygen vacancies at CeO<sub>2</sub> (111): critical role of hydroxyls, Phys. Rev. Lett. 116 (2016) 1–6, https://doi.org/10.1103/ PhysRevLett.116.086102.
- [37] P.K. Huttunen, D. Labadini, S.S. Hafiz, S. Gokalp, E.P. Wolff, S.M. Martell, M. Foster, DRIFTS investigation of methanol oxidation on CeO<sub>2</sub> nanoparticles, Appl. Surf. Sci. 554 (2021), 149518, https://doi.org/10.1016/j. apsusc.2021.149518.
- [38] C. Schilling, A. Hofmann, C. Hess, M. Vero, Raman spectra of polycrystalline CeO<sub>2</sub>: a density functional theory study, J. Phys. Chem. C 121 (2017) 20834–20849, https://doi.org/10.1021/acs.jpcc.7b06643.
- [39] A. Filtschew, K. Hofmann, C. Hess, Ceria and its defect structure: new insights from a combined spectroscopic approach, J. Phys. Chem. C 120 (2016) 6694–6703, https://doi.org/10.1021/acs.jpcc.6b00959.
- [40] G. Jacobs, R.A. Keogh, B.H. Davis, Steam reforming of ethanol over Pt/ceria with co-fed hydrogen, J. Catal. 245 (2007) 326–337, https://doi.org/10.1016/j. icat.2006.10.018.
- [41] Q. Wang, K. Lun, M.A. Bañares, Operando Raman-online FTIR investigation of ceria, vanadia/ceria and gold/ceria catalysts for toluene elimination, J. Catal. 364 (2018) 80–88, https://doi.org/10.1016/j.jcat.2018.05.001.
- [42] S. Besselmann, E. Loffler, On the role of monomeric vanadyl species in toluene adsorption and oxidation on V2O5 r TiO2 catalysts: a Raman and in situ DRIFTS study, (2000).
- [43] N. Hirata, S. Suga, Y. Noguchi, M. Shibuta, H. Tsunoyama, T. Eguchi, A. Nakajima, Highly Ordered self-assembled monolayers of carboxy- and ester- terminated alkanethiols on Au (111): infrared absorption and hyperthermal-deposition experiments with Cr (benzene) 2 lons. (2017). 10.1021/acs.jpcc.7b00292.
- [44] C. Scirè, R.G. Urso, D. Fulvio, G.A. Baratta, M.E. Palumbo, Mid-IR band strength, density, refractive index, and thermal evolution study for solid CH<sub>2</sub>DOH pure and in astrophysical relevant mixtures, Spectrochim. Acta Part A Mol. Biomol. Spectrosc. 219 (2019) 288–296, https://doi.org/10.1016/j.saa.2019.04.021.
- [45] A.M. Nadeem, G.I.N. Waterhouse, H. Idriss, The reactions of ethanol on TiO2 and Au/TiO2 anatase catalysts, 182 (2012) 16–24. 10.1016/j.cattod.2011.08.051.
- [46] G.N. Vayssilov, M. Mihaylov, P.S. Petkov, K.I. Hadjiivanov, K.M. Neyman, Reassignment of the vibrational spectra of carbonates, formates, and related surface species on ceria: a combined density functional and infrared spectroscopy investigation, J. Phys. Chem. C 115 (2011) 23435–23454, https://doi.org/ 10.1021/jp.2080502
- [47] S.M. Lee, Y.H. Lee, D.H. Moon, J.Y. Ahn, D.D. Nguyen, S.W. Chang, S.S. Kim, Reaction mechanism and catalytic impact of Ni/CeO<sub>2-x</sub> catalyst for lowtemperature CO<sub>2</sub> methanation, Ind. Eng. Chem. Res. 58 (2019) 8656–8662, https://doi.org/10.1021/acs.iecr.9b00983.
- [48] L. Lin, S. Yao, Z. Liu, F. Zhang, N. Li, D. Vovchok, A. Mart, R. Castan, J. Lin, S. D. Senanayake, D. Su, D. Ma, J.A. Rodriguez, *In situ* characterization of Cu/CeO<sub>2</sub> nanocatalysts for CO<sub>2</sub> hydrogenation: morphological effects of nanostructured ceria on the catalytic activity, J. Phys. Chem. C. 122 (2018) 12934–12943, https://doi.org/10.1021/acs.jpcc.8b03596.
- [49] S. Krishnamoorthy, J.A. Rivas, M.D. Amiridis, Catalytic Oxidation of 1,2-Dichlorobenzene over, Support. Trans. Metal Oxides 272 (2000) 264–272, https://doi. org/10.1006/jcat.2000.2895.
- [50] P. Uznanski, E. Bryszewska, Synthesis of silver nanoparticles from carboxylate precursors under hydrogen pressure, J. Mater. Sci. 45 (2010) 1547–1552, https://doi.org/10.1007/s10853-009-4122-3.
- [51] K.D. Dobson, A.J. McQuillan, In situ infrared spectroscopic analysis of the adsorption of aliphatic carboxylic acids to TiO<sub>2</sub>, ZrO<sub>2</sub>, Al<sub>2</sub>O<sub>3</sub>, and Ta<sub>2</sub>O<sub>5</sub> from aqueous solutions, Spectrochim. Acta Part A Mol. Biomol. Spectrosc. 55 (1999) 1395–1405, https://doi.org/10.1016/S1386-1425(98)00303-5.
- [52] X. Fu, L. Guo, W. Wang, C. Jia, K. Wu, R. Si, L. Sun, C. Yan, Direct identification of active surface species for the water—gas shift reaction on a gold—ceria catalyst, J. Am. Chem. Soc. 141 (2019) 4613–4623, https://doi.org/10.1021/jacs.8b09306.
- [53] R. Leppelt, B. Schumacher, V. Plzak, M. Kinne, R.J. Behm, Kinetics and mechanism of the low-temperature water–gas shift reaction on Au/CeO<sub>2</sub> catalysts in an idealized reaction atmosphere, J. Catal. 244 (2006) 137–152, https://doi.org/ 10.1016/j.jcat.2006.08.020.
- [54] Y. Cui, Z. Li, Z. Zhao, V.J. Cybulskis, K.D. Sabnis, W. Han, V. Ortalan, W. F. Schneider, J. Greeley, W. Nicholas, F.H. Ribeiro, Participation of interfacial hydroxyl groups in the water-gas shift reaction over Au/MgO catalysts, Catal. Sci. Technol. 7 (2017) 5257–5266, https://doi.org/10.1039/c7cy01020f.
- [55] I. Fishtik, R. Datta, A UBI–QEP microkinetic model for the water–gas shift reaction on Cu(111), Surf. Sci. 512 (2002) 229–254, https://doi.org/10.1016/S0039-6028 (02)01689-8.
- [56] T. Kropp, J. Paier, J. Sauer, Interactions of Water with the (111) and (100) Surfaces of Ceria, J. Phys. Chem. C 121 (2017) 21571–21578, https://doi.org/10.1021/acs. jpcc.7b08150.
- [57] A. Badri, C. Binet, J. Lavalley, An FTIR study of surface ceria hydroxy groups during a redox process with H<sub>2</sub>, J. Chem. Soc. Faraday Trans. 92 (1996) 4669–4673, https://doi.org/10.1039/FT9969204669.

- [58] H. Zhu, Y. Li, X. Zheng, In-situ DRIFTS study of CeO<sub>2</sub> supported Rh catalysts for N<sub>2</sub>O decomposition, Appl. Catal. A Gen 571 (2019) 89–95, https://doi.org/ 10.1016/j.apcata.2018.12.020.
- [59] N.C. Nelson, J. Sebastia, A.D. Sadow, S.H. Overbury, Selective hydrogenation of phenol catalyzed by palladium on high-surface-area ceria at room temperature and ambient pressure, Catalysis 5 (2015) 2051–2061, https://doi.org/10.1021/ cs502000i
- [60] J.M. Lopez, A.L. Gilbank, T. García, B. Solsona, S. Agouram, L. Torrente-murciano, The prevalence of surface oxygen vacancies over the mobility of bulk oxygen in nanostructured ceria for the total toluene oxidation, Appl. Catal. B Environ. 174–175 (2015) 403–412, https://doi.org/10.1016/j.apcatb.2015.03.017.
- [61] J. Carrasco, G. Vile, D. Ferna, Molecular-level understanding of CeO<sub>2</sub> as a catalyst for partial alkyne hydrogenation, J. Phys. Chem. C 118 (2014) 5352–5360, https:// doi.org/10.1021/jp410478c.
- [62] T. Montini, M. Melchionna, M. Monai, P. Fornasiero, Fundamentals and catalytic applications of CeO<sub>2</sub>-based materials, Chem. Rev. 116 (2016) 5987–6041, https:// doi.org/10.1021/acs.chemrev.5b00603.
- [63] Y. Wang, C. Wo, IR spectroscopic investigations of chemical and photochemical reactions on metal oxides: bridging the materials gap, Chem. Soc. Rev. 46 (2017) 1875–1932, https://doi.org/10.1039/C6CS00914J.

- [64] C. Yang, F. Bebensee, A. Nefedov, C. Wöll, T. Kropp, L. Komissarov, C. Penschke, R. Moerer, J. Paier, J. Sauer, Methanol adsorption on monocrystalline ceria surfaces, J. Catal. 336 (2016) 116–125, https://doi.org/10.1016/j. icat.2016.01.003.
- [65] A. Siokou, R.M. Nix, Interaction of methanol with well-defined ceria surfaces: reflection/absorption infrared spectroscopy, X-ray photoelectron spectroscope, and temperature-programmed desorption study, J. Phys. Chem. B. 103 (1999) 6984–6997, https://doi.org/10.1021/jp991127h.
- [66] N.G. Hamilton, A.P. Amrute, J. Pe, Understanding CeO<sub>2</sub> as a deacon catalyst by probe molecule adsorption and *in situ* infrared characterisations, Phys. Chem. Chem. Phys. 15 (2013) 3454–3465, https://doi.org/10.1039/c2cp42767b.
- [67] D.R. Mullins, P.M. Albrecht, T. Chen, F.C. Calaza, M.D. Biegalski, H.M. Christen, S. H. Overbury, Water dissociation on CeO<sub>2</sub> (100) and CeO<sub>2</sub> (111), Thin Films 2 (2012) 19419–19428, https://doi.org/10.1021/jp306444h.
- [68] B. Chen, Y. Ma, L. Ding, L. Xu, Z. Wu, Q. Yuan, Reactivity of hydroxyls and water on a CeO<sub>2</sub> (111) thin film surface: the role of oxygen, Vacancy 2 (2013) 5800–5810, https://doi.org/10.1021/jp312406f.